

Dual energy computed tomography for the head

Norihito Naruto¹ · Toshihide Itoh² · Kyo Noguchi¹ 

Received: 14 September 2017 / Accepted: 29 October 2017 / Published online: 9 November 2017
© Japan Radiological Society 2017

Abstract Dual energy CT (DECT) is a promising technology that provides better diagnostic accuracy in several brain diseases. DECT can generate various types of CT images from a single acquisition data set at high kV and low kV based on material decomposition algorithms. The two-material decomposition algorithm can separate bone/calcification from iodine accurately. The three-material decomposition algorithm can generate a virtual non-contrast image, which helps to identify conditions such as brain hemorrhage. A virtual monochromatic image has the potential to eliminate metal artifacts by reducing beam-hardening effects. DECT also enables exploration of advanced imaging to make diagnosis easier. One such novel application of DECT is the X-Map, which helps to visualize ischemic stroke in the brain without using iodine contrast medium.

Keywords Dual energy CT · Dual source CT · Head · Bone removal · Monoenergetic image · Brain hemorrhage · X-Map

Introduction

Although the concept of dual energy (DE) was first conceived in the late 1970s, it was not broadly implemented in the clinic [1]. After a quarter-century, the first practical dual

energy CT (DECT) with several clinical applications was commercially released onto the market in the early 2000s [2]. DECT is unique because two data sets are acquired simultaneously at two different X-ray energies. This may allow materials to be decomposed into such clinically relevant materials as bone/calcification, iodine, and water/tissue, for instance, even if they show similar CT values in Hounsfield units using single X-ray energy CT [3, 4].

Recently, the DE applications have been increasing for various clinical conditions. These are classified into two types of algorithms in principle: the two-material decomposition (2MD) algorithm and the three-material decomposition (3MD) algorithm. The 2MD algorithm can distinguish bone/calcification from other materials, and can be used for direct bone removal in CT angiography or CT venography [4–9]. The 3MD algorithm can computationally generate a virtual non-contrast image by eliminating the iodine component from the image. In patients with brain hemorrhage, it is used to differentiate iodine and hemorrhage or acute ischemic stroke after intra-arterial recanalization [5, 6, 9–11]. A virtual monoenergetic image shows clinically important properties by increasing contrast enhancement at lower energies [12], and reducing beam-hardening artifacts from high-density objects such as skull bone or a metallic clip at higher energies [13].

Technical aspects of DECT

Material decomposition algorithm

The material decomposition (MD) algorithm is a method to generate images using DECT, which can decompose a material into two or three prior known materials using each absorption property [14, 15]. The MD algorithm can be

✉ Kyo Noguchi
kyo@med.u-toyama.ac.jp

¹ Department of Radiology, Graduate School of Medicine and Pharmaceutical Science, University of Toyama, 2630 Sugitani, Toyama 930-0194, Japan

² Department of Research and Collaboration, Siemens Healthcare, Tokyo, Japan

measured or visualized in analogy with the vector analysis using an orthogonal diagram with high-kV CT values on the x -axis and low-kV CT values on the y -axis. Any voxel coordinate in this diagram can be represented in terms of two material-specific vectors for the 2MD algorithm and three material-specific vectors for the 3MD algorithm. The voxel can then be decomposed into the two- or three-material vectors and each vector length represents the amount of each material in the voxel.

2MD algorithm

The 2MD is a basic algorithm on DECT that can distinguish between two different clusters corresponding to different materials such as bone and iodine, for instance (Fig. 1a). A typical application of 2MD for the head is DE direct bone removal in a contrast or non-contrast-enhanced scan.

3MD algorithm

The 3MD algorithm is an extension of the 2MD algorithm. This algorithm can decompose a voxel of the material into three different materials (i.e., fat, tissue, and iodine), and it is thus often used to generate an iodine distribution map from a contrast-enhanced scan data set (Fig. 1b). Because iodine shows relatively strong absorption compared to other tissue components in a body, an iodine-specific vector can be created independently from other material-specific vectors. The iodine slopes therefore represent the relative contrast enhancement at each voxel originally along the line connecting the two materials (i.e., fat and soft-tissue), and the length of each iodine slope also represents the amount of iodine in each voxel. Therefore, the 3MD algorithm can generate an iodine distribution map as well as a virtually computed non-contrast image consisting of all voxels along the line between fat and soft-tissue (virtual non-contrast image). This is used for DE applications in brain hemorrhage.

Virtual monoenergetic imaging algorithm

Virtual monoenergetic imaging (VMI) is known to be useful to manipulate iodine contrast enhancement retrospectively. The algorithm is based on the 2MD with two materials such as iodine or bone and water. Once decomposition is complete it allows computation of a simulated image at any X-ray energy between 40 and 190 keV.

VMI is often used for two purposes in the head. One purpose is to improve iodine contrast enhancement. Because of a characteristic of iodine's mass attenuation coefficient, the iodine enhancement is increased at a lower keV and this phenomenon yields an optimal image with the best enhancement, noise, contrast-to-noise ratio (CNR) or lesion detectability. VMI at lower keV settings could significantly increase

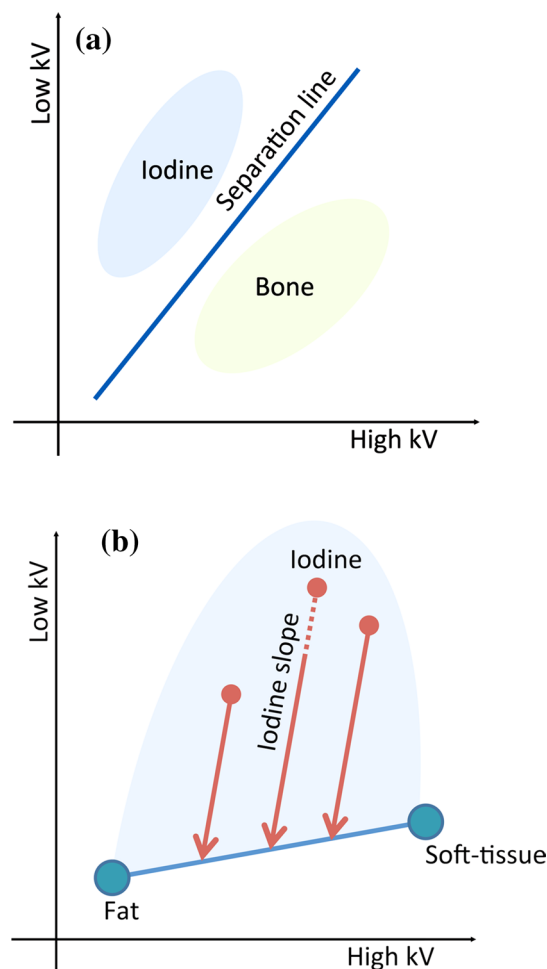


Fig. 1 The MD is the algorithm that generates several DE images. The 2MD algorithm (a) can distinguish one material from other materials such as bone and iodine using a separation line. This algorithm has been used for the DE direct bone removal application. The 3MD algorithm (b) can extract the iodine component from contrast-enhanced tissues. All voxels are projected along the iodine-specific slope to the line connecting fat and soft-tissue. This algorithm has been used for DE brain hemorrhage application

the iodine contrast enhancement as well as the CNR because iodine shows a larger absorption near its k-edge (approximately 33 keV). A freely selectable keV setting provides a near-optimal image in terms of signal strength and noise properties that works well for ischemic stroke or intra-cerebral hemorrhage/tumor diagnosis.

The other purpose of VMI is to reduce artifacts from metallic implants such as platinum coils or clips, so-called metal-artifact-reduction. A higher keV contributes to reduced beam-hardening artifacts between high-attenuation objects. One of the major causes of the artifacts from metallic implants is the beam hardening effect of the X-ray spectrum, which results from the strong absorption characteristics of metals; thus, increasing the energy levels in order to reduce the beam hardening effects helps to reduce

artifacts from metals. A tube voltage of 150 kV or Sn150 kV (150 kV with tin filtration) correspond to X-ray energies less than 100 keV, so that VMI at a higher keV setting, such as 100 keV, provides an advantage in reducing metal artifacts [12, 13] (Fig. 2).

Clinical applications of DECT

General applications of DECT for the head

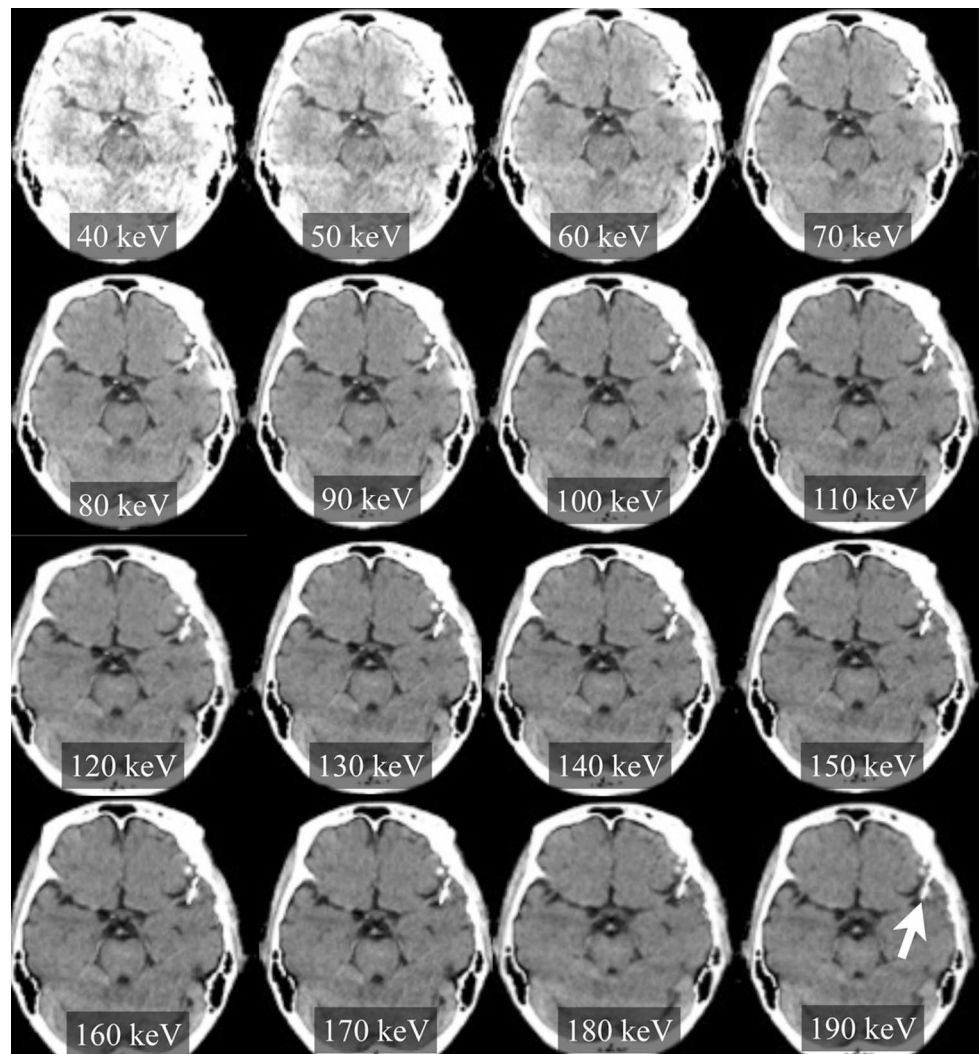
As described in the previous section, DECT provides several unique applications for the head. In this section, the focus is on three DECT applications and their usefulness in routine practice in: (1) in brain hemorrhage, (2) direct bone removal and (3) virtual monoenergetic application. Additionally, the utility of the originally acquired images at 80 kV and Sn150 kV as well as the DE simulated

standard CT image which is the synthetically generated standard 120 kV image by linear combination of 80 kV and Sn150 kV, will also be discussed.

DE brain hemorrhage

DE brain hemorrhage is an application to visualize small fresh hemorrhages from contrast-enhanced images using the 3MD algorithm for cerebrospinal fluid, hemorrhage, and iodine. This application has near-perfect accuracy in differentiating intracranial hemorrhage from iodinated contrast extravasation or staining and may be particularly helpful in patients who have an aneurysm with subarachnoid hemorrhage, tumor bleeding with intracranial hemorrhage, arteriovenous malformation with intracranial hemorrhage, or acute ischemic stroke after intra-arterial recanalization (IAR) [6–10, 16, 17].

Fig. 2 A patient with a left aneurysm of the middle cerebral artery (MCA). Surgical treatment including aneurysm clipping of aneurysm was performed. VMI from 40 to 190 keV in 10-keV steps obtained at 80 kV and Sn150 kV. High keV images show reduced artifacts surrounding the clip (*arrow*)



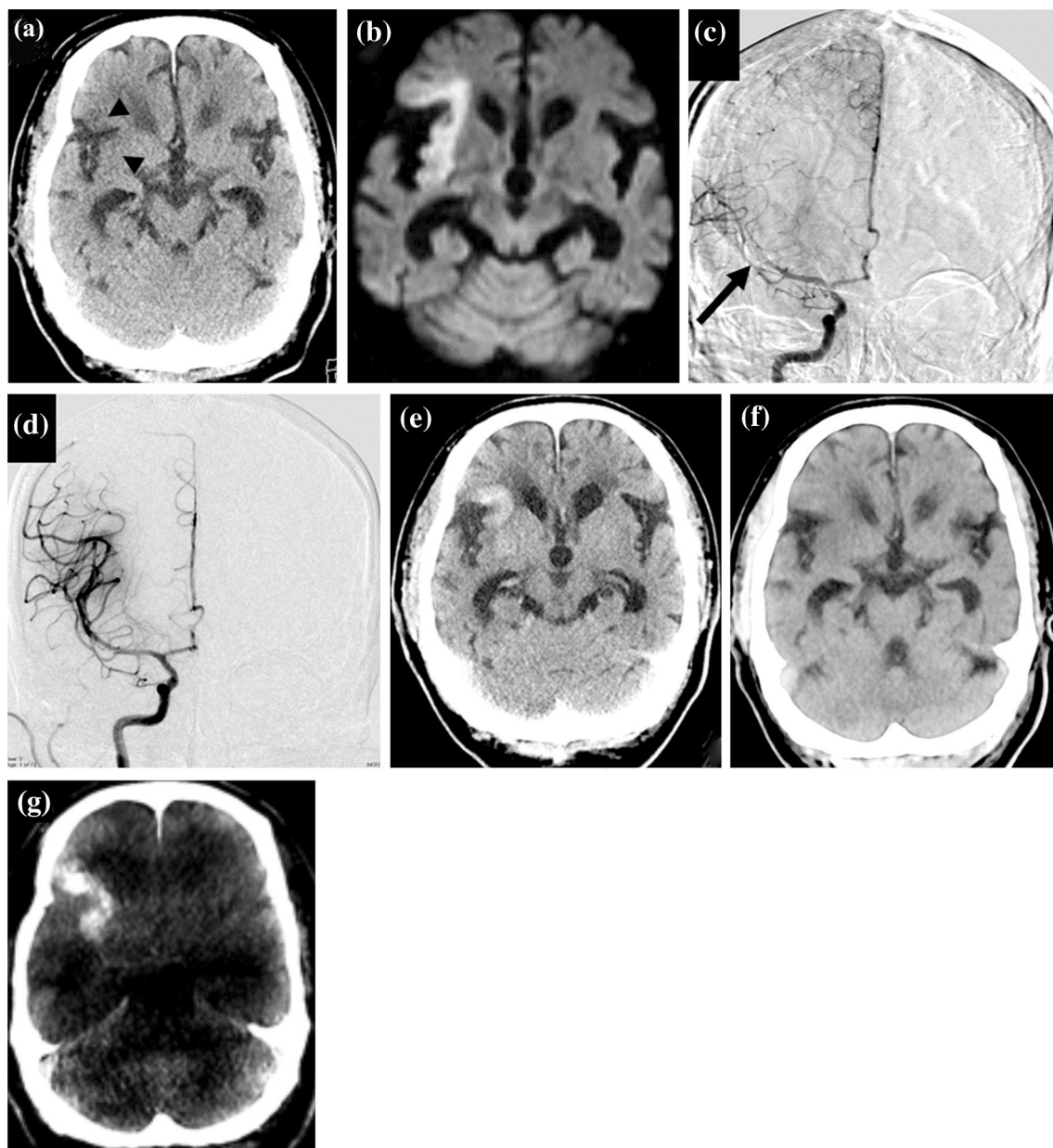


Fig. 3 A patient with acute ischemic stroke underwent IAR. Simulated standard CT (a) reconstructed from DECT shows gray-white matter differentiation in the frontal lobe and a loss of the insular ribbon sign (*arrow heads*) because of right middle cerebral artery (MCA) occlusion. The diffusion-weighted image (b) shows hyperintensity in the right frontal lobe and insular. Before IAR, DSA (c) identifies the right MCA occlusion (*arrow*). After IAR, DSA (d)

shows that the MCA occlusion was recanalized. Simulated standard CT (e) after intra-arterial therapy shows hyper-density in the cortex of the right MCA territory. Virtual non-contrast image (f) reconstructed from DECT shows hypo-density. Iodine overlay image (g) reconstructed from DECT shows hyper-density and this is considered to be contrast material extravasation

Evaluation of IAR

Recently, intravenous therapy with IAR for acute ischemic stroke has gained increasing attention. In the Prolyse in Acute Cerebral Thromboembolism (PROACT) study, the IAR technique was considered acceptable and appropriate therapy for acute ischemic stroke [18]. However, one of

the major complications is intra-cerebral hemorrhage and extravasations of iodinated contrast material. Extravasations of iodinated contrast material may increase the CT densities of intra-cerebral hemorrhage to rather high levels after IAR. Even though the contrast enhancement on CT after IAR is not associated with hemorrhagic complications and the extravasations of iodinated contrast material is considered

to be a negative prognostic sign, it is important to detect the presence or absence of hemorrhage, and it is then necessary to distinguish the hemorrhage from extravasations of iodinated contrast material [11]. DE brain hemorrhage helps to distinguish intra-cerebral hemorrhage from iodinated contrast material (Fig. 3).

DE direct bone removal

DE direct bone removal can help to distinguish vessels from bone or calcified plaques using the 2MD algorithm for bone and iodine. The DE direct bone removal application is a reliable and faster method compared to the simple subtraction method with unenhanced and enhanced scanning using single-energy CT.

CT-angiography and CT-venography

DECT provides advantages for CT-angiography (DECTA) and CT-venography (DECTV) in terms of radiation dose reduction and reliable bone removal compared to conventional CTA. Although conventional CTA needs two independent scans, a non-contrast scan and a contrast-enhanced scan, DECTA and DECTV require only a single acquisition to complete, making it possible to avoid an unnecessary radiation dose and concerns about image-processing, such as inaccurate subtraction and segmentation that are caused by motion artifacts between two scans. Watanabe, et al. first reported on the usefulness of DECTA with DE direct bone removal [7]. Several authors have also reported that DECTA and DECTV with DE direct bone removal are powerful tools for evaluating intracranial vessels, aneurysms, and cerebral

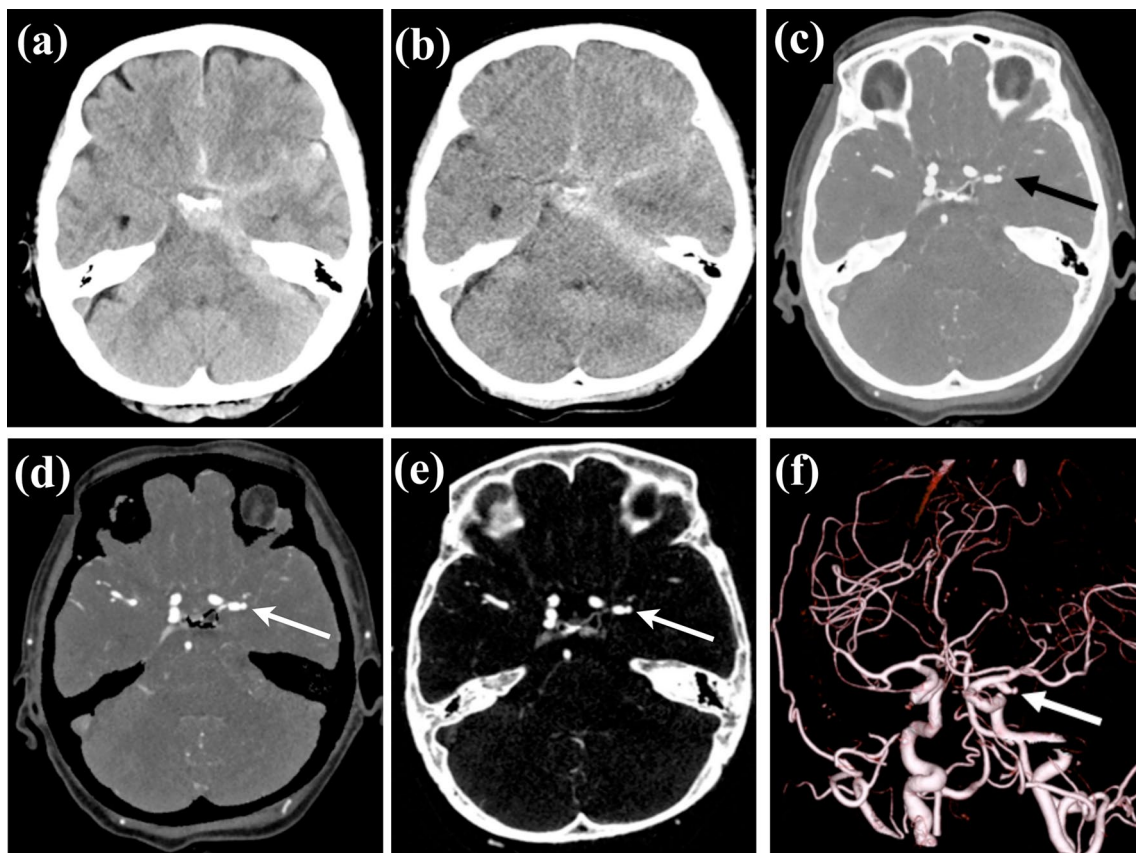


Fig. 4 A patient with subarachnoid hemorrhage resulting from an aneurysm rupture. Non-contrast standard CT (a) shows subarachnoid hemorrhage in the basal cisterns and left sylvian vallicula. Virtual non-contrast image (b) reconstructed from DECTA shows subarachnoid hemorrhage in the basal cistern, but the noise level is slightly increased compared with the standard image. Simulated standard CT (c) and bone removal images with DE application (d) show an aneu-

rysm of the left internal carotid-posterior communicating artery (IC-PC aneurysm) (arrow). The iodine overlay image (e) shows enhanced vessels (arrow) without the density of the surrounding hemorrhage. Volume rendering image from DECTA using the DE bone removal application (f) shows an IC-PC aneurysm with an exact outline and its relationship to the parent vessels (arrow)

venous thrombosis (Fig. 4) [5, 6, 8, 19]. However, DE direct bone removal may overestimate the calcified stenosis lesion, particularly in a small vessel, because of the blooming artifact of calcification compared with digital subtraction angiography (DSA) [7].

Carotid artery calcification

It has been recognized that morphology and composition of atherosclerotic plaques in carotid vessels is a risk factor of ischemic stroke. Even though DSA is considered to be the gold standard technique for the quantification of internal carotid artery stenosis, DE bone removal application provides comparable information to DSA in a faster and easier manner (Fig. 5) [4, 5, 19, 20].

Advantage of DE direct bone removal application in non-enhanced scans

Generally, it is difficult to detect small intracranial hemorrhages near the skull. Non-contrast CT with DE direct bone removal can improve the prominence of small intracranial hemorrhages, particularly those adjacent to the bone, by removing bone that can interfere with the visualization of acute hemorrhage (Fig. 6) [21]. In diagnosing deep venous thrombosis and sinus venous thrombosis, non-contrast CT is often performed in an emergency setting in most institutions. The thrombotic object increases its attenuation in the affected vessels for the first week after onset. It has been reported that non-contrast CT provides insufficient diagnosis for a cortical venous thrombosis compared to deep venous

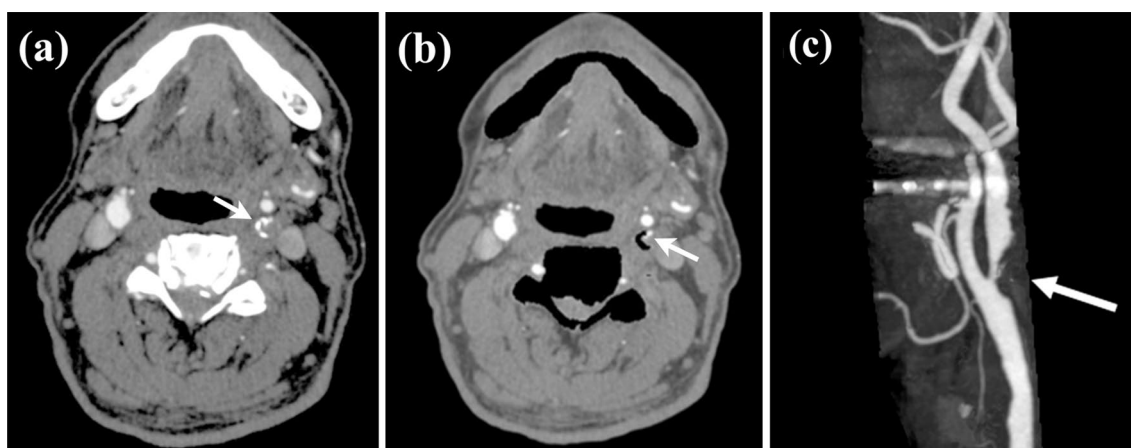
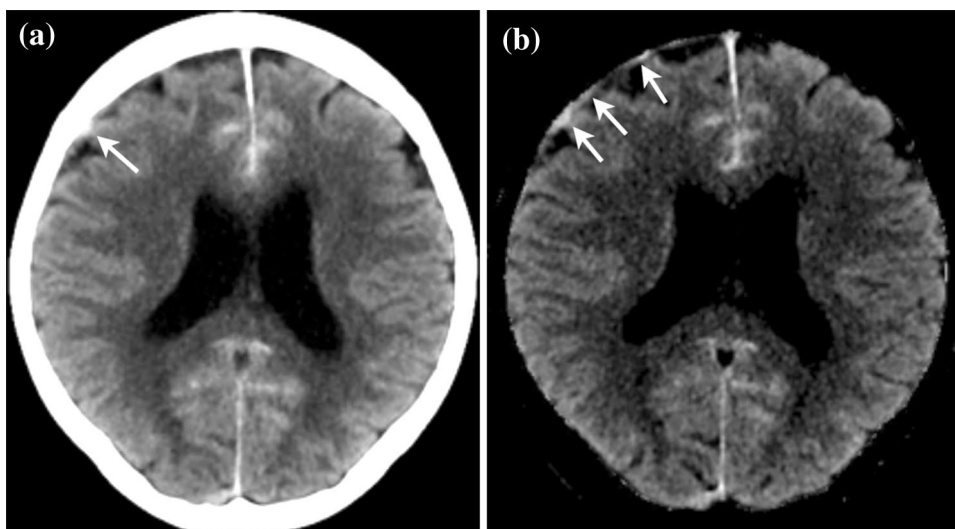


Fig. 5 A patient with severe stenosis of the left proximal internal carotid artery (ICA). DECTA (a) shows severe stenosis of the left proximal internal carotid artery caused by hard and soft plaques. The hard plaque is adjacent to the ICA with luminal stenosis. DECTA

with an automatic hard plaque removal (b) better describes the degree of luminal stenosis (arrow) than DECTA without hard plaque removal (a). A maximum intensity projection image (c) shows a clear visualization of the ICA

Fig. 6 A patient with acute subarachnoid hemorrhage resulting from a ruptured aneurysm of the anterior communicating artery, and small right frontal subdural hematomas resulting from head trauma. A simulated standard CT image (a) clearly shows the acute subarachnoid hemorrhage. It is difficult to detect the small right frontal acute subdural hemorrhage (arrow) adjacent to bone. The DE-bone removal image (b) clearly shows the acute subarachnoid hemorrhage and the small right frontal acute subdural hemorrhage (arrows)



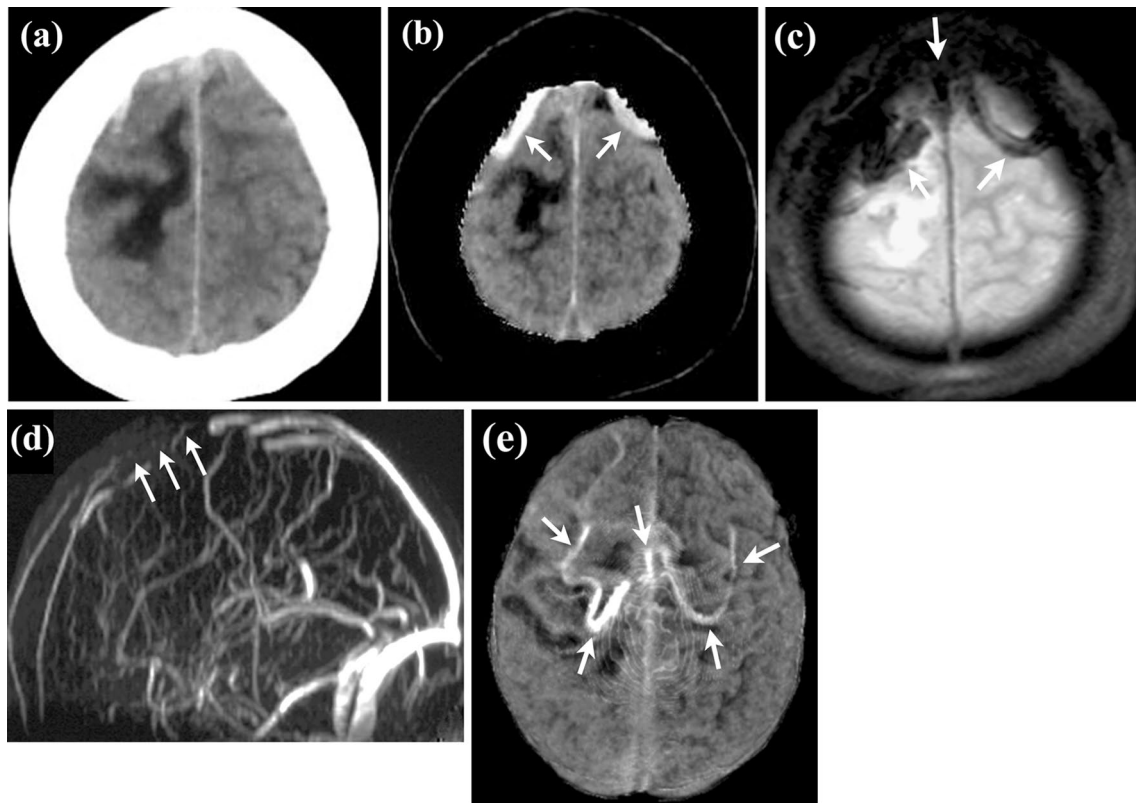


Fig. 7 A patient with thrombosis of the superior sagittal sinus (SSS) and both cortical veins. It is difficult to detect cortical venous thrombosis on a simulated standard image (a) of non-contrast DECT. The DE bone removal image (b) and T2*-weighted image (c) clearly show acute thrombosis of cortical veins and SSS (arrows). MR

venography (d) shows occlusion of the SSS (arrows). A volume rendering image of the DE bone removal image (e) clearly shows acute thrombosis of the SSS and both cortical veins as hyper-dense vessel lesions (arrows)

thrombosis [22, 23]. In contrast, DE bone removal CT helps to identify both cerebral venous sinus thrombosis and cortical venous thrombosis that are located adjacent to the bone (Fig. 7).

Utility of original acquisition images

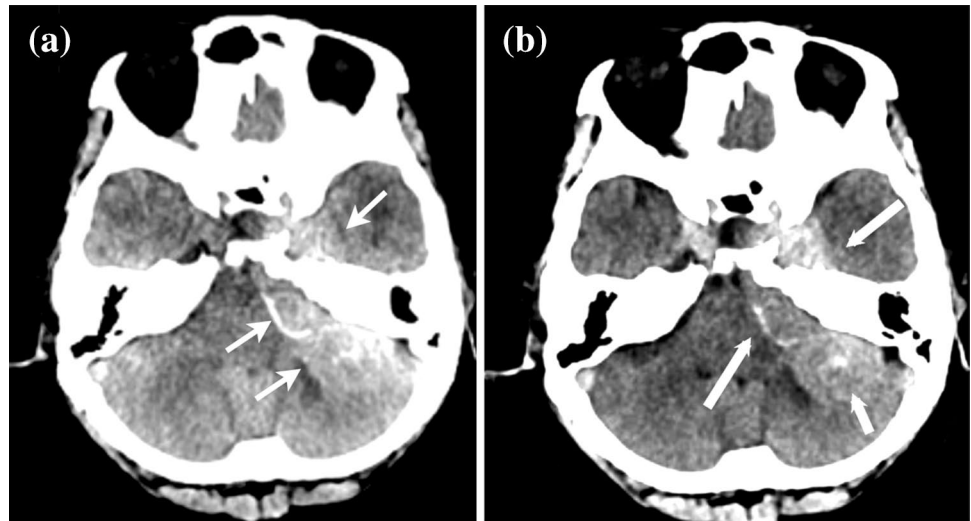
A DE simulated standard CT image is generated by a weighted linear combination of two acquired images such as 80 kV and Sn150 kV. By adjusting the weight, a DE simulated standard CT image may have characteristics of a standard 120 kV image in terms of pixel noise and CT values, and therefore DE simulated standard CT images are used alternatively to make a diagnosis.

On the other hand, both low-kV (80 kV) and high-kV (Sn150 kV) images are also utilized for diagnosis respecting each characteristic. A significant advantage of 80-kV images is that they provide relatively higher CNR in a vascular study, and it is possible to reduce the amount of iodine

contrast material. Acquisition at Sn150 kV is expected to give fewer beam hardening artifacts from high-density objects such as bones, and helps to lower beam hardening artifacts in the images at the posterior or middle fossa levels. Often observed shadow-like artifacts over brain tissue near the bone-brain interface can be reduced using a Sn150-kV tube voltage setting. The image at Sn150 kV helps to diagnose a hyper-dense sign for acute cerebral infarction as well as cerebral hemorrhage or a tumor near a complex bone structure region (Fig. 8).

A reason for this may be because tin filtration is used at high kV. Tin filtration set up below an X-ray tube at high kV (Sn150 kV) selectively reduces the X-ray photons in the lower energy range so that the spectral shape of 150 kV becomes narrower and its peak shifts to a higher energy range [24, 25]. Therefore, the effective incident X-ray energy of 150 kV increases by approximately 25 keV. Thus, the spectral separation between low kV (80 kV) and high kV (Sn150 kV) becomes larger, which allows more accurate DECT acquisition.

Fig. 8 A patient with meningioma. It is difficult to detect the edge of the tumor in the 80-kV image (a) because of beam-hardening artifacts (arrows), but in the Sn150-kV image (b), the tumor is easily detected (arrows)



Future directions and challenges

As mentioned above, DECT has already been used as a useful diagnostic tool for head conditions or brain diseases in daily practice. However, it is still necessary to explore further areas for its application. One such potential application is X-Map, which we are the first to report and have developed an X-Map algorithm in order to visualize cerebral ischemia in non-contrast DECT [26].

X-Map algorithm

An early ischemic sign on non-contrast CT is known to be useful for identifying irreversibly damaged tissues, and it describes features such as loss of gray-white matter differentiation, obscuration of the lentiform nucleus, and loss of insular ribbon [27, 28]. However, skill and experience are required to determine these signs.

X-Map is a virtual gray matter map that can emphasize the attenuation difference between brain parenchyma and water content. The brain parenchyma mainly consists of three materials: gray matter, white matter and water. A basic assumption here regarding a difference between the gray matter and the white matter is a fractional difference in the lipid content in these voxels. When the difference in the lipid content in white matter using 3MD is suppressed, a virtual gray matter map is generated. Theoretically, there is only a fractional difference between the two voxel contents, which are gray matter and water. Because edema progression may increase the water content in a voxel, the X-Map can distinguish a lesion with an increase in water content and identify it as a hypo-dense lesion using the virtual gray matter map.

In a diagram of the X-Map algorithm (Fig. 9), it is assumed that the brain parenchyma mainly consists of

three materials: gray matter, white matter and water. The X-Map emphasizes water content as a hypo-dense lesion in the brain parenchyma by suppressing a difference in the lipid content between the white matter and the gray matter. It projects all voxels plotted in the diagram along the lipid-specific slope of 2.0 at 80 kV and Sn150 kV settings onto the baseline that is connected between the nominal

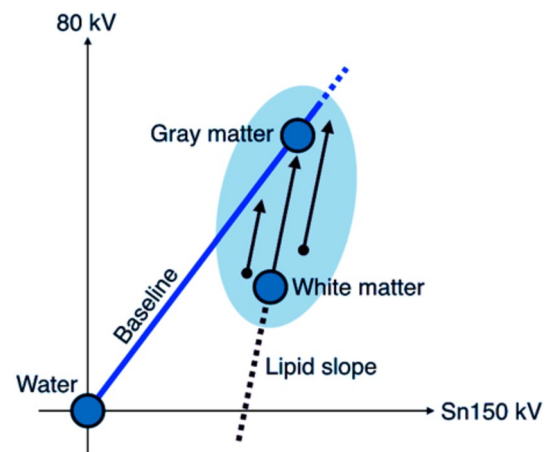


Fig. 9 The X-Map uses a modified 3MD algorithm. A motivation of this application is to visualize an ischemic change of the brain parenchyma by detecting an increase in water content in a voxel. To identify a small change in water content, the 3MD algorithm had a lipid-specific slope of 2.0 applied in order to suppress the small difference in the lipid content in gray and white matter. As shown in the diagram, the nominal values of gray matter and white matter are 33 HU at Sn150 kV and 42 HU at 80 kV, and 29 HU at Sn150 kV and 34 HU at 80 kV, respectively. The lipid-specific slope between the nominal point of gray matter and white matter is 2.0 using the third generation DSCT (SOMATOM Force; Siemens Healthcare, Forchheim, Germany)

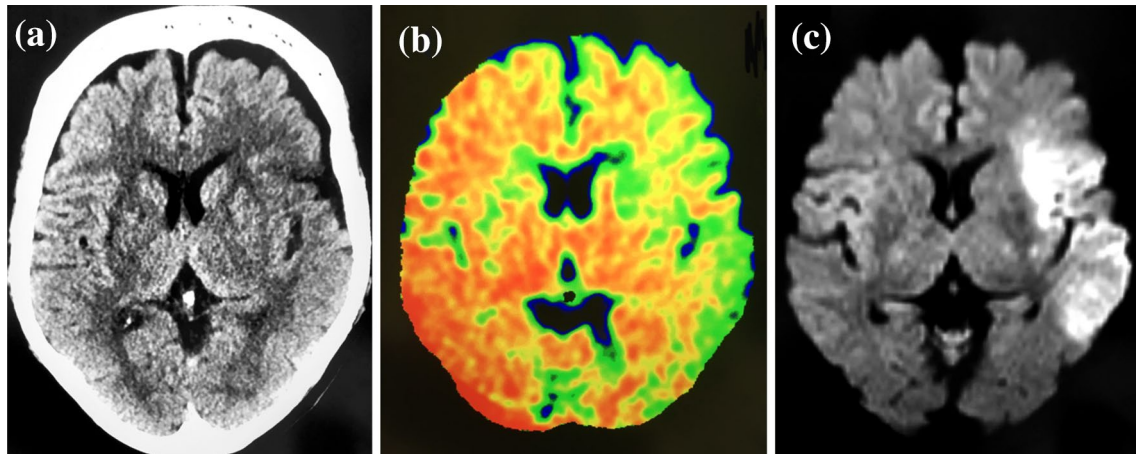
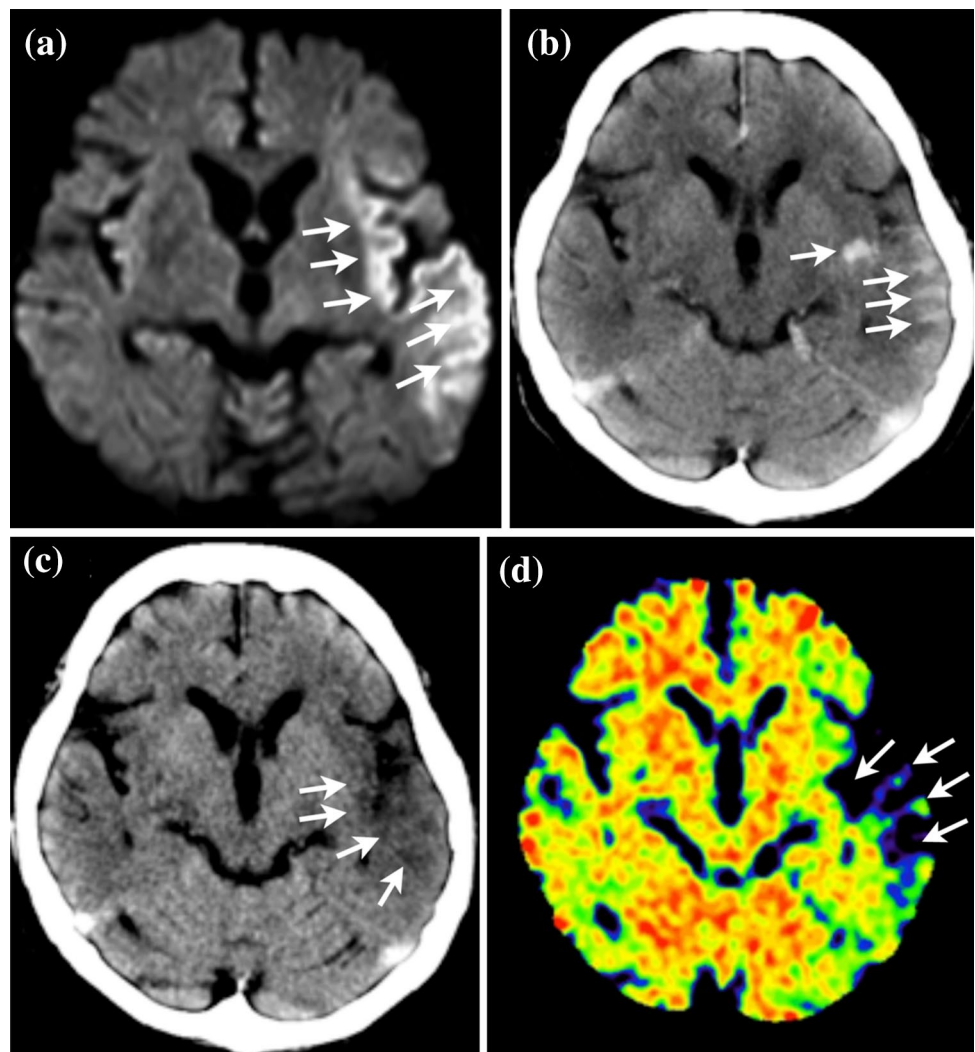


Fig. 10 A patient with acute ischemic stroke 3 h after onset. A simulated standard CT image (a) obtained 3 h after the ischemic stroke onset shows no definite early ischemic change, although the left frontoparietal operculum may show questionable hypo-density. The

X-Map (b) clearly shows the ischemic lesion in the left middle cerebral artery territory. The diffusion-weighted image (c) also shows a definite acute ischemic lesion in the left MCA territory

Fig. 11 A patient with acute ischemic stroke who underwent IAR. A diffusion-weighted image (a) before IAR shows hyper-intensity in the left insular and temporal lobe (arrows). Simulated standard CT (b) after IAR shows hyper-density in the insular and temporal lobe (arrows). A virtual non-contrast image (c) reconstructed from DECT shows hypo-density (arrows) and it is considered to be contrast material extravasation. The X-Map (d) clearly shows the early ischemic lesion in the left insular and temporal lobe (arrows) compared with the virtual non-contrast image (c)



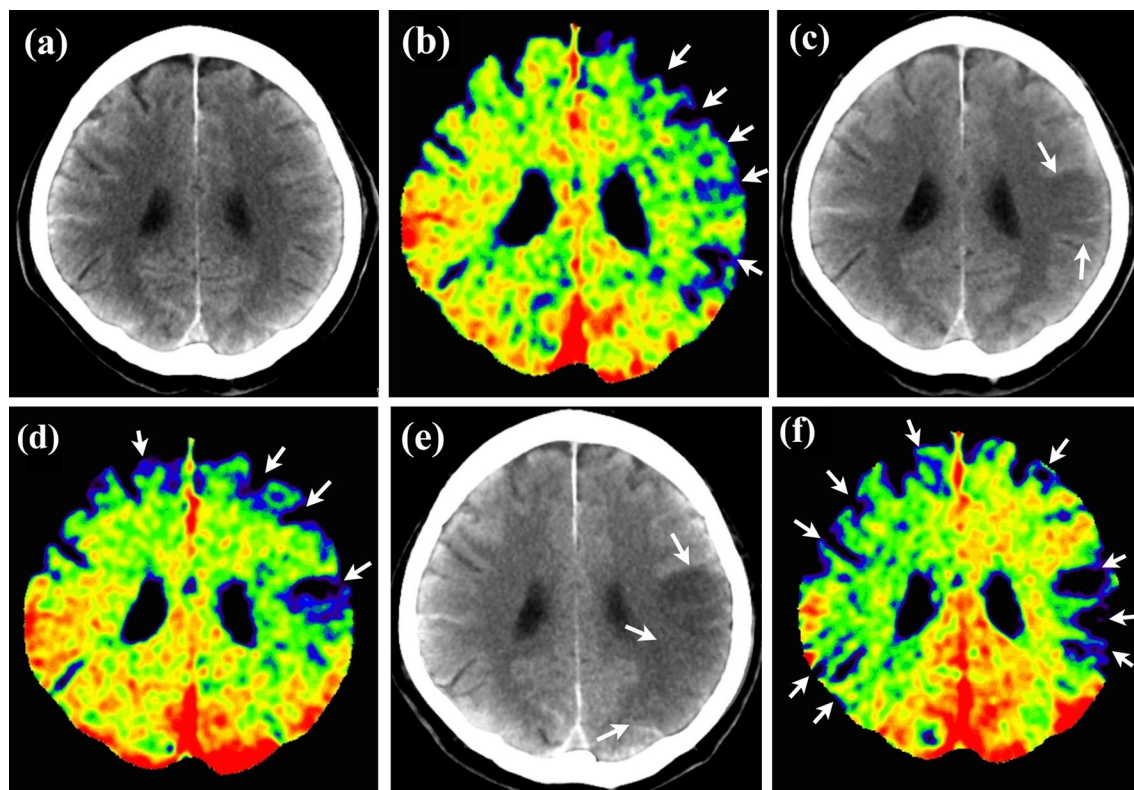


Fig. 12 A patient with acute subarachnoid hemorrhage who underwent therapy. Aphasia occurred in the afternoon of day 8 after subarachnoid hemorrhage. A simulated standard CT (a) does not show the abnormality, but the X-Map (b) suggests an abnormality in the left hemisphere (arrows). The aphasia became worse in the morning

of day 9. A simulated standard CT (c) and X-Map (d) show a definite edema in the left hemisphere (arrows). Left hemiparesis also occurred in the afternoon of day 9. A simulated standard CT (e) does not show an abnormality in the right hemisphere, but the X-Map (f) suggests an abnormality in the right hemisphere (arrows)

point of water and the nominal point of gray matter (33 HU at Sn150 kV and 42 HU at 80 kV). This mathematical operation can generate the virtual gray matter map and all relevant voxels in the brain parenchyma are placed on the baseline. Therefore, the voxels with increasing edema containing a large fraction of water content will be located rather far from the nominal point of gray matter and closer to the nominal point of water on the baseline [26].

X-Map is a powerful tool to supplement a simulated standard CT to characterize acute ischemic lesions (Figs. 10, 11, 12). Two independent studies showed promising results of the X-Map algorithm. One study (our study) [26] compared the X-Map with DWI acquired 30–60 min after DECT. The study found that acute infarctions delineated by the X-Map agreed very well with those by diffusion-weighted images, including ischemic regions that recovered after treatments. Another study [29] compared X-Map (brain edema image) with conventional CT using a 24-h follow-up CT as the gold standard. Mohammed et al. called these processed images brain edema images. However, it is the X-Map merely explained in a

different way. Although pixel values were projected onto *not* the GM line but the *water–air line*, resulting values reflect the relative position on the projected line; therefore brain edema images were X-Map images that were scaled by a constant. It showed that the X-Map (brain edema image) is able to detect edema and measure the end-infarct (core infarct) volume more accurately than conventional CT does. The sensitivity, specificity, positive predictive value, and negative predictive value of the X-Map (brain edema image) were 93.3, 100, 100, and 91.7%, respectively, while those of conventional CT were 80, 72.7, 80, and 72.7%, respectively [29].

Despite these promising results, there are the following two problems with the X-Map. First, DECT images have smearing artifacts near the brain–skull boundary. Second, X-Map values have large inter-patient and intra-patient variations. The X-Map fixes the base line. However, gray matter values have inter-patient and intra-patient variations. These problems may cause false positive or false negative findings. Therefore, the original X-Map cannot

replace the simulated standard CT for the diagnosis of acute ischemic stroke at this time.

Conclusion

DECT can separate materials using a MD algorithm, analyzing the difference in the CT value at two different energies. DECT is a powerful tool for supplementing simulated standard CT for characterizing intracranial lesions. Application to brain hemorrhage can distinguish contrast material from a hemorrhage. The bone removal application can remove bone and calcification without subtraction. The bone removal application is also useful for detecting acute intracranial hemorrhagic lesions such as small subdural, epidural, or contusional hematomas and acute venous thrombosis. A monoenergetic imaging application can choose the most suitable kV image in making a diagnosis. The new DECT map “X-Map” may have great potential in supplementing simulated standard CT to characterize brain lesions without using contrast agents.

Acknowledgements The authors would like to thank Mati Ur Rehman, PhD, Department of Radiology for English proofreading of this manuscript.

Author contributions N. Naruto: clinical studies, data acquisition, manuscript preparation. T. Itoh: definition of intellectual content, manuscript review. K. Noguchi: guarantor of integrity of the entire study, manuscript editing, manuscript review.

Compliance with ethical standards

Conflict of interest The authors declare that they have no conflicts of interest.

Ethical statement We declare that all human studies have been approved by the institutional review board of the University of Toyama and have therefore been performed in accordance with the ethical standards laid down in the 1964 Declaration of Helsinki and its later amendments. No written informed consent was required for the retrospective analysis of clinically acquired data.

References

- Brooks RA. A quantitative theory of the Hounsfield unit and its application to dual energy scanning. *J Comput Assist Tomogr*. 1977;1:487–93.
- Flohr TG, McCollough CH, Bruder H, et al. First performance evaluation of a dual-source CT (DSCT) system. *Eur Radiol*. 2006;16:256–68.
- Johnson TR. Dual-energy CT. General principles. *AJR Am J Roentgenol*. 2012;1(99):S3–8.
- McCollough CH, Leng S, Yu L, et al. Dual-and multi-energy CT: principles, technical approaches, and clinical applications. *Radiology*. 2015;276:637–53.
- Postma AA, Das M, Stadler AA, et al. Dual energy CT: what the neuroradiologist should know. *Curr Radiol Rep*. 2015;3:16.
- Postoma AA, Hofman PA, Stadler AA, et al. Dual-energy CT of the brain and intracranial vessels. *AJR Am J Roentgenol*. 2012;199:S26–33.
- Watanabe Y, Uotani K, Nakazawa T, et al. Dual-energy direct bone removal CT angiography for evaluation of intracranial aneurysm or stenosis: comparison with conventional digital subtraction angiography. *Eur Radiol*. 2009;19:1019–24.
- Schulz B, Kuehling K, Kromen W, et al. Automatic bone removal technique in whole-body dual-energy CT angiography: performance and image quality. *AJR Am J Roentgenol*. 2012;199:W646–50.
- Gupta R, Phan CM, Leidecker C, et al. Evaluation of dual-energy CT for differentiating intracerebral hemorrhage from iodinated contrast material staining. *Radiology*. 2010;257:205–11.
- Hu R, Besheli LD, Young J, et al. Dual-energy head CT enables accurate distinction of intraparenchymal hemorrhage from calcification in emergency department patients. *Radiology*. 2016;280:177–83.
- Yoon W, Seo JJ, Kim JK, et al. Contrast enhancement and contrast extravasation on computed tomography after intra-arterial thrombolysis in patients with acute ischemic stroke. *Stroke*. 2004;35:876–81.
- Yu L, Leng S, McCollough CH. Dual energy CT-based monochromatic imaging. *AJR Am J Roentgenol*. 2012;199:S9–15.
- Bamberg F, Dierks A, Nikolaou K, et al. Metal artifact reduction by dual energy computed tomography using monoenergetic extrapolation. *Eur Radiol*. 2011;21:1424–9.
- Johnson TR, Kraus B, Sedlmair M, et al. Material differentiation by dual energy CT: initial experience. *Eur Radiol*. 2007;17:1510–7.
- Liu X, Yu L, Primak AN, et al. Quantitative imaging of element composition and mass fraction using dual-energy CT: three-material decomposition. *Med Phys*. 2009;36:1602–9.
- Phan CM, Yoo AJ, Hirsch JA, et al. Differentiation of hemorrhage from iodinated contrast in different intracranial compartments using dual-energy head CT. *AJNR Am J Neuroradiol*. 2012;33:1088–94.
- Kim SJ, Lim HK, Lee HY, et al. Dual-energy CT in the evaluation of intracerebral hemorrhage of unknown origin: differentiation between tumor bleeding and pure hemorrhage. *AJNR Am J Neuroradiol*. 2012;33:865–72.
- Furlan A, Higashida R, Wechsler L, et al. Intra-arterial pro-urokinase for acute ischemic stroke: PROACT II study: a randomized controlled trial. *JAMA*. 1999;282:2003–11.
- Thomas C, Korn A, Krauss B, et al. Automatic bone and plaque removal using dual energy CT for head and neck angiography: feasibility and initial performance evaluation. *Eur J Radiol*. 2010;76:61–7.
- Vlahos I, Chung R, Nair A, et al. Dual-energy CT: vascular applications. *AJR Am J Roentgenol*. 2012;199:S87–97.
- Naruto N, Tannai H, Nishikawa K, et al. Dual-energy bone removal computed tomography (BRCT): preliminary report of efficacy of acute intracranial hemorrhage detection. *Emerg Radiol*. 2017;. <https://doi.org/10.1007/s10140-017-1558-7> (Epub ahead of print).
- Vijay RK. The cord sign. *Radiology*. 2006;240:299–300.
- Linn N, Pfeifferkorn T, Ivanicova K, et al. Noncontrast CT in deep cerebral venous thrombosis and sinus thrombosis: comparison of its diagnostic value for both entities. *AJNR Am J Neuroradiol*. 2009;30:728–35.
- Primak AN, Giraldo JCR, Eusemann CD, Schmidt B, Kantor B, Fletcher JG, McCollough CH. Dual-source dual-energy CT with additional tin filtration: dose and image quality

- evaluation in phantoms and in vivo. *AJR Am J Roentgenol.* 2010;195:1164–74.
25. Primak AN, Ramirez Giraldo JC, Liu X, Yu L, McCollough CH. Improved dual-energy material discrimination for dual-source CT by means of additional spectral filtration. *Med Phys.* 2009;36:1359–69.
 26. Noguchi K, Itoh T, Naruto N, et al. A novel imaging technique (X-Map) to identify acute ischemic lesions using noncontrast dual-energy computed tomography. *J Stroke Cerebrovasc Dis.* 2017;26:34–41.
 27. Tomura N, Uemura K, Inugami A, et al. Early CT finding in cerebral infarction: obscuration of the lentiform nucleus. *Radiology.* 1988;168:463–7.
 28. Truwit CL, Barkovich AJ, Marton G, et al. Loss of the insular ribbon: another early CT sign of acute middle cerebral artery infarction. *Radiology.* 1990;176:801–6.
 29. Mohammed MF, Marais O, Min A, et al. Unenhanced dual-energy computed tomography: visualization of brain edema. *Invest Radiol.* 2017;. <https://doi.org/10.1097/RLI.0000000000000413> (**Epub ahead of print**).